BNL-71739-2003-CP

Preliminary results from a simulation of quenched QCD with overlap fermions on a large lattice*†

F. Berruto[a], N. Garron[b], C. Hoelbling[b], L. Lellouch[b], C. Rebbi[c] and N. Shoresh[c]

[a]Department of Physics, Brookhaven National Laboratory, Upton NY 11973, USA

[b]Centre de Physique Théorique‡, Case 907, CNRS Luminy, F-13288 Marseille Cedex 9, France

[c]Department of Physics, Boston University, 590 Commonwealth Avenue, Boston MA 02215, USA

We simulate quenched QCD with the overlap Dirac operator. We work with the Wilson gauge action at $\beta = 6$ on an $18^3 \times 64$ lattice. We calculate quark propagators for a single source point and quark mass ranging from $am_q = 0.03$ to 0.75. We present here preliminary results based on the propagators for 60 gauge field configurations.

1. Introduction

The closely related domain wall [1,2] and overlap [3–5] formulations of lattice fermions, with their ability to preserve chiral symmetry even at finite lattice spacing [6,7], offer an almost ideal tool for lattice QCD calculations. Still overlap or domain wall fermions can only be implemented at a high computational cost. Thus it is important to perform exploratory calculations on large lattices in order to validate the applicability of these novel formulations. At the same time, large scale QCD simulations with overlap or domain wall fermions, because of the benefits of chiral symmetry, can produce valuable cross-checks of observables calculated with more traditional quark discretizations, or even permit the evaluation of observables otherwise out of the reach of practical calculations. In earlier studies we simulated quenched QCD with overlap fermions on a $16^3 \times 32$ lattice, obtaining results for the pseudoscalar spectrum, strange quark mass and quark condensate [8,9], for the kaon B parameter [10,11] and for non-perturbative renormalization constants [9–11]. Although the results of this earlier work turned out to be quite satisfactory, the size of the lattice, especially its extent in time, were found insufficient for the calculation of some observables. For example, the plateaus needed to isolate the K mesons in the calculation of B_K extended for only two lattice spacings and we could not reliably evaluate vector meson masses and decay constants or baryon masses. This prompted us to extend our overlap calculations to a larger system. It is important to observe that increasing the size of the lattice in simulations with overlap fermions does not only entail an augmentation of the (already quite heavy) computational cost. Indeed, since the calculation of the overlap operator requires the use of some suitable approximation to the inverse square root of a very large sparse matrix, the increase of the size of the matrix may produce serious problems of convergence. For these reasons, and also in consideration of the computational resources available to us, we decided to use a lattice of size $18^3 \times 64$, with double the extent in time, but only a moderate increase in the spatial extent with respect to our former calculation. Thus we generated and archived 100 $18^3 \times 64$ pure gauge field configurations with the Wilson gauge action at $\beta = 6$. We used a 6-hit Metropolis algorithm, tuning the acceptance to ≈ 0.5, performed 11,000 initial equilibrating iterations, after which 10,000 iterations were done between each pair of subsequent configurations. From a measurement of Wilson loops we determined $r_0/a = 5.36 \pm 0.11$ for the Sommer scale defined by $r_0^2 F(r_0) = 1.65$. With $r_0 = 0.5$fm we get $a^{-1} = 2.11 \pm 0.04$GeV.

For each of the above configurations we cal-

*Work supported in part by US DOE grants DE-FG02-91ER40676 and DE-AC02-98CH10866, EU HPP contracts HPRN-CT-2000-00145 and HPRN-CT-2002-00311, and grant HPMF-CT-2001-01468. We thank Boston University and NCSA for use of their supercomputer facilities.

†Combined presentations by C. Hoelbling, L. Lellouch and C. Rebbi at *Lattice 2003*, Tsukuba, Japan.

‡ Unité Propre de Recherche 7061.

culated quark propagators with the overlap Dirac operator, with $\rho = 1.4$, for a single point source and all 12 color-spin combinations, for $am_q = 0.03, 0.04, 0.06, 0.08.0.1, 0.25, 0.5, 0.75$. For brevity we do not reproduce here the formula for the overlap Dirac operator: we refer to [8,9] for the relevant equations and selected citations. The results we present here are based on the analysis of 60 configurations. For the calculation of the overlap operator (more properly, of its action on a given vector) for the first 55 configurations we used the Zolotarev approximation with 12 poles, after Ritz projection of the lowest 12 eigenvectors of H^2. We found, however, the Chebyshev approximation to be computationally less costly (by approximately 20%) and therefore we are now using this approximation. With both approximations we impose $|D^\dagger D\psi - \chi|^2 < 10^{-7}$ as convergence criterion. We project out the lowest 12 eigenvectors of H^2 also with the Chebyshev approximation and use the evaluation of the next highest eigenvalue to set the required degree of the expansion, which typically varies between 100 and 500. Our code has been written in F90 with OMP directives and we have been running in shared memory mode on 16 and 32 processor IBM-P690 nodes at Boston University and NCSA.

To conclude this section, we would like to mention that other large scale quenched QCD calculations with overlap fermions have been presented in [12–15].

2. Light hadron spectrum and quark condensate

Our first concern has been to verify that the results with the new, larger lattice are compatible with the values found for the observables in our former calculations [8,9] and that the measurement of the observables can be extended to the much larger temporal extent with reliable statistics. We present here a sample of these checks.

In Fig. 1 we report the new results for the ratio

$$\rho(t) = G_{\nabla_0 A_0 P}(t)/G_{PP}(t) \qquad (1)$$

where $G_{IJ}(t)$, $IJ = \nabla_0 A_0 P, PP$, are non-singlet zero-momentum, 2-point functions made from the bilinears I and J. On account of the axial Ward identity, $\rho(t)$ should be constant in time. The

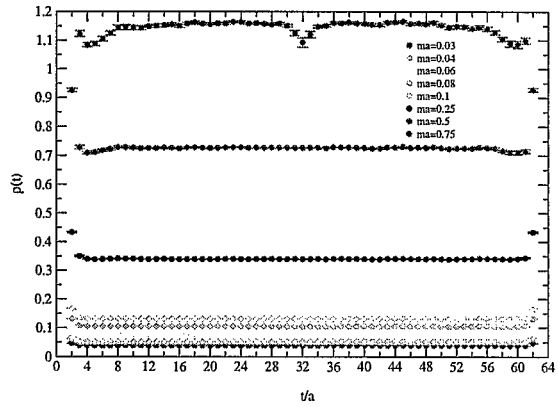

Figure 1. Results for the axial Ward identity.

figure shows that $\rho(t)$ can be reliably measured over the entire extent of the lattice for all quark mass values and is indeed constant in time. The

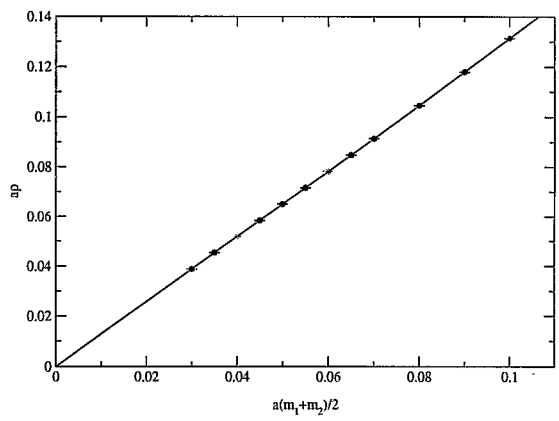

Figure 2. The ratio ρ of Eq. 1 as function of quark mass.

fit $\rho = A + a(m_1 + m_2)/Z_A + C(am_1 + am_2)^2$ (see Fig. 2) gives $A = -(0.96 \pm 3.35) \times 10^{-5}, Z_A = 1.554 \pm 0.001$ [1.55 ± 0.04], $C = (6.87 \pm 0.18) \times 10^{-2}$. The numbers in square brackets, here and in the following, indicate results we found in [8,9].

Figure 3 illustrates the value of the effective mass from the (0-momentum component of the) correlation functions of the pseudoscalar density, of the pseudoscalar minus scalar densities and of

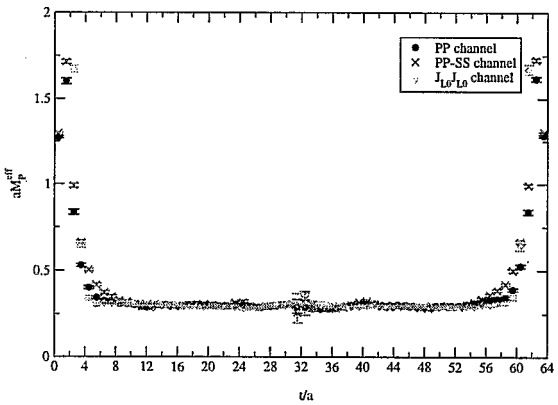

Figure 3. Effective pseudoscalar mass plateaus for $am_q = 0.06$.

the temporal component of the left-handed currents, for $am_q = 0.06$. We see that the signal for the correlation functions extends through the whole lattice. These three correlation func-

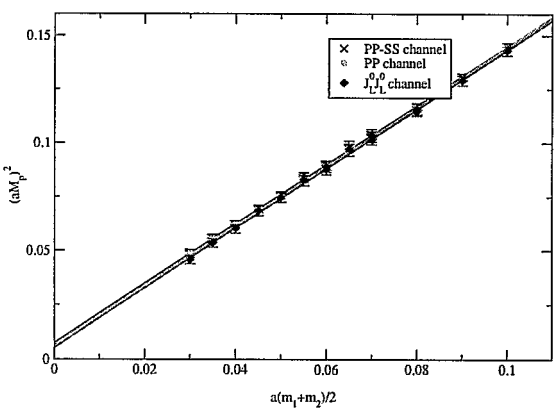

Figure 4. Pseudoscalar mass squared as function of the total quark mass.

tions, symmetrized with respect to $t \to 64a - t$, have been fit in the range $12 \leq t/a \leq 32$, and Fig. 4 displays the values thus found for the pseudoscalar mass as well as the linear fit $(aM_P)^2 = A + Ba(m_1 + m_2)/2$ which gives

$$\begin{aligned}
\mathrm{PP} : A &= (6.69 \pm 1.76) \times 10^{-3},\ B = 1.38 \pm 0.02 \\
\mathrm{PP-SS} : A &= (7.27 \pm 2.44) \times 10^{-3},\ B = 1.37 \pm 0.02 \\
\mathrm{J_L^0, J_L^0} : A &= (5.31 \pm 2.58) \times 10^{-3},\ B = 1.38 \pm 0.04 \\
[\mathrm{PP} : B &= 1.39 \pm 0.03;\ \ \mathrm{PP-SS} : B = 1.43 \pm 0.07]
\end{aligned}$$

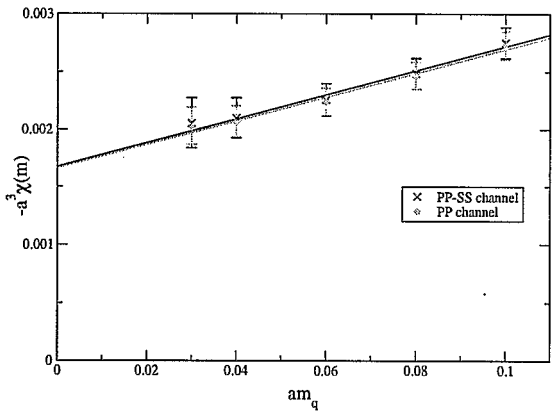

Figure 5. Determination of the chiral condensate.

Figure 5 shows the results for the scalar condensate from the Gell-Mann, Oakes and Renner relation, for degenerate quark masses, together with the linear fit $\chi = A + Bam_q$, which gives

$$\begin{aligned}
\mathrm{PP} : A &= (1.66 \pm 0.18) \times 10^{-3} \\
B &= (1.03 \pm 0.15) \times 10^{-2} \\
\mathrm{PP-SS} : A &= (1.67 \pm 0.24) \times 10^{-3} \\
B &= (1.04 \pm 0.21) \times 10^{-2} \\
[\mathrm{PP-SS} : A &= (1.17 \pm 0.27) \times 10^{-3}]
\end{aligned}$$

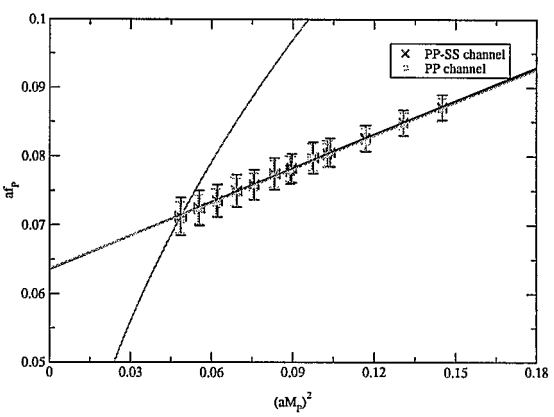

Figure 6. Determination of a.

Finally, we reproduce in Fig. 6 the determination of a with the method of lattice physical planes: the red line corresponds to the physical ratio F_K/M_K with $M_K = 0.495\,\mathrm{GeV}$ $F_K = 0.16\,\mathrm{GeV}$. We find $a^{-1} = 2.238 \pm 0.083\,\mathrm{GeV}$ from

the PP channel and $a^{-1} = 2.236 \pm 0.098[2.29 \pm 0.09]$ GeV from the PP-SS channel.

Figures 7, 8 illustrate new results, which were out of reach with a smaller lattice. In Fig. 7 we show the quantity $\log|G_{BB}(t)|$ with $B \equiv B_{\pm} = (1 \pm \gamma_0)\epsilon_{abc}\left[u_a^T C\gamma_5 d_b\right] u_c$ (a sum over the spatial coordinates of B over the time slice at t is implicit). Since the correlation function with the $1+\gamma_0$ projector describes forward propagating $1/2^+$ baryons and backward propagating $1/2^-$ baryons, while the two parities are interchanged with the $1-\gamma_0$ projector, in Fig. 7 we plot the $1-\gamma_0$ correlation function against $64a - t$. The results for the two correlation functions, after this inversion of the time axis, are quite consistent, as one would expect, and exhibit an extended linear region over which one can extract an estimate of the lowest baryon masses. The corresponding linear fits are also shown in Fig. 7.

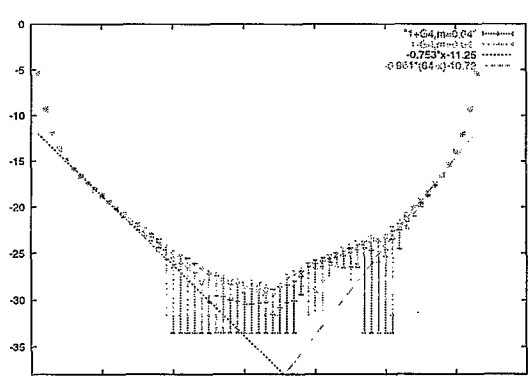

Figure 7. Logarithm of the baryon-baryon correlation functions.

In Fig. 8 we collect all of our results for the lowest $1/2^+$ and $1/2^-$ baryon masses. We calculated the masses corresponding to all combinations where two of the quarks have the same mass. The masses of the $1/2^+$ states appear to fall on a single curve, indicating a dependence only on the total quark mass. The masses of the $1/2^-$ seem to indicate a dependence on the quark mass difference also, but the statistical errors are high and a more elaborated analysis should be done before deriving any such implication from the data. We emphasize that these results are preliminary. In

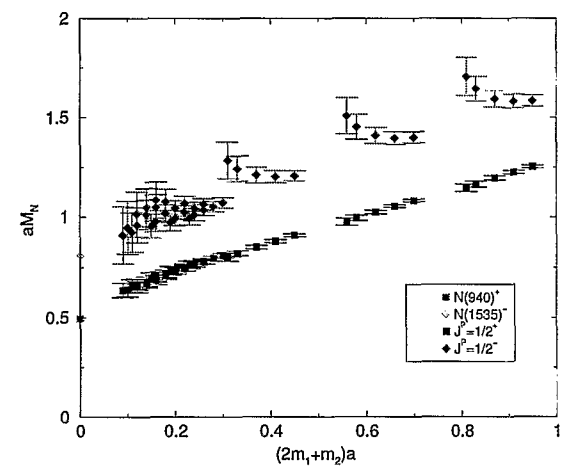

Figure 8. Baryon masses as function of the total quark mass.

particular the masses in Fig. 8 have been obtained with point sources *and* sinks. While having calculated point source quark propagators forces us to use point sources, we should be able to improve the statistical significance of the results by using suitable extended sink operators. Calculations along these lines are in progress.

3. Experimenting with the charm quark

In the present section we investigate the behavior of overlap fermions with heavy quarks Q for which $am_Q \not\ll 1$. In particular, we are interested in understanding whether the charm quark can be approximately simulated at lattice spacings of around 2 GeV, where the charm has a bare mass $am_c \sim 0.75$. Related results, obtained with a different gauge action, can be found in [16].

Though a rigorous investigation of discretization errors would require simulations at a number of values of the lattice spacing, at the present time we only have a simulation for which $a^{-1} \sim 2$ GeV. We have thus devised a number of tests which provide us with some measure of the mass-dependent discretization errors present in our simulation. They concern a variety of quantities, some of which are of direct phenomenological interest such as the leptonic decays constant of the D_s meson, f_{D_s}.

3.1. Axial and vector Ward identities

We turn once again to the non-singlet axial (AWI) and vector (VWI) Ward identities. Instead of working with the ratio $\rho(t)$ defined in Eq. (1), we consider the quantity

$$\mathcal{Z}_A(t; m_1, m_2) \equiv \frac{(am_1 + am_2)}{\rho(t; m_1, m_2)} , \qquad (2)$$

with a similar definition for $\mathcal{Z}_V(t; m_1, m_2)$ in terms of vector currents and scalar densities. These quantities are also constant in time, by virtue of the AWI and VWI, and reduce to the renormalization constants Z_A and Z_V of the axial and vector currents in the chiral limit. $\mathcal{Z}_A(t)$ and $\mathcal{Z}_V(t)$ have very nice plateaus in t for all quark-mass combinations, though error bars and fluctuations on $\mathcal{Z}_V(t)$ are substantially larger. We thus fit them to a constant in the time range $14 \leq at \leq 50$, thereby obtaining mass-dependent "renormalization constants" $Z_A(m_1, m_2)$ and $Z_V(m_1, m_2)$. The fits to $\mathcal{Z}_A(t)$ are all excellent, except for the mass combination $am_1 = am_2 = 0.75$ where there is some evidence that the signal is lost for a handful of points around the center of the lattice (cf. Fig. 1). The situation is much less satisfactory for $\mathcal{Z}_V(t)$, where the fluctuations make it difficult to obtain reliable fits.

The quantities $Z_{A,V}(m_1, m_2)$ are of particular interest here, because their mass dependence is solely due to discretization errors. Given our definition, the leading mass dependence is of the form $a^2(m_1 + m_2)$ and $a^2(m_1 - m_2)^2/(m_1 + m_2)$. In Fig. 9 we plot $Z_A(m_1, m_2)/Z_A(0, 0)$ as a function of $(am_1 + am_2)$ for all mass combinations, were $Z_A(0, 0)$ is obtained as described below. We consider $Z_V(m_1, m_2)$ only for $(am_1 + am_2) \leq 0.2$, since it is not clear that we can reliably fit $\mathcal{Z}_V(t)$ for larger masses. The values of $Z_A(m_1, m_2)$ for $(am_1 + am_2) \leq 0.2$ display linear behavior, indicating that mass-dependent discretization errors are dominated by $a^2(m_1 + m_2)$-type terms in this range of masses. Therefore, in this mass range we fit $Z_A(m_q, m_q)$ to:

$$Z_A(m_q, m_q) = Z_A(0, 0)\,(1 + 2(aB)(am_q)) \ , \quad (3)$$

where we only consider degenerate combinations to eliminate possible $a^2(m_1 - m_2)^2/(m_1 + m_2)$ terms. We find $Z_A(0, 0) = 1.5544(15)$, which is entirely compatible with the value given after Eq. (1), and $aB = -0.102(5)$.

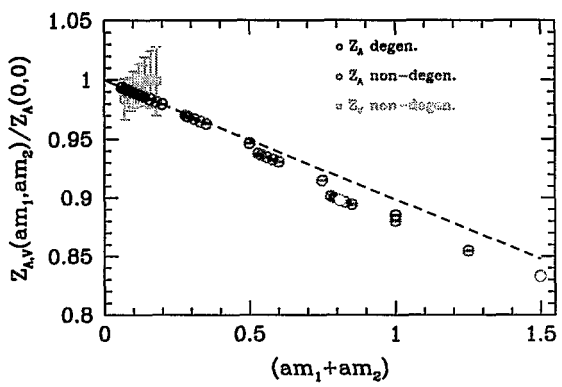

Figure 9. $Z_{A,V}(m_1, m_2)/Z_A(0, 0)$ vs. $(am_1 + am_2)$. The straight line corresponds to the fit described around Eq. (3). The two filled symbols approximately correspond, from left to right, to a D_s and an η_c meson.

The first point worth noting is that the coefficient B of the $a^2(m_1 + m_2)$ discretization error is small, $B \sim 225\,\text{MeV}$. The second interesting feature is that deviation from linearity becomes statistically significant (i.e. larger than 3 standard deviations) only for $(am_1 + am_2) \gtrsim 0.28$. We are actually able to consistently fit $Z_A(m_1, m_2)$ all the way up to $am_1 = am_2 = 0.5$ with the addition of two terms proportional to $a^3(m_1 + m_2)^2$ and $a^2(m_1 - m_2)^2/(m_1 + m_2)$, and all the way up to $am_1 = am_2 = 0.75$ with an additional term proportional to $a^4(m_1 + m_2)^3$, though the coefficients obtained in the latter fit are only marginally consistent with those from our two other fits. In these fits to extended mass ranges, we further find that the coefficients of the higher order terms are approximately one half to a full order of magnitude smaller than aB. The net result is that discretization errors inferred from $Z_A(m_1, m_2)$ are approximately 10% at $(am_1, am_2) = (0.06, 0.75)$ and 15% at $(am_1, am_2) = (0.75, 0.75)$, mass combinations which corresponds roughly to a D_s and an η_c meson, respectively. Moreover, chiral symmetry seems to be good, as evidenced by the compatibility of $Z_A(m_1, m_2)$ and $Z_V(m_1, m_2)$ at small

masses. Thus, there is no evidence for a major breakdown of overlap fermions up to $am_q = 0.75$ and $(am_1 + am_2) = 1.5$.

3.2. 2-point functions, pseudoscalar meson masses and decay constants

We have performed fits to the zero-momentum PP, $PP{-}SS$, A_0P, PA_0, A_0A_0 and $J_0^L J_0^L$ correlators, all of which have the pseudoscalar meson as the lightest contributing state. The fit form used is:

$$\sum_{\mathbf{x}} \langle I(x)J(0)\rangle \stackrel{ax_0 \gg 1}{\longrightarrow} \frac{\mathcal{Z}_{IJ}}{2M_{IJ}}\left[e^{-M_{IJ}x_0} + s_{IJ}e^{-M_{IJ}(T-x_0)}\right], \tag{4}$$

where the fit parameters are $\mathcal{Z}_{IJ}$ and M_{IJ}, and $s_{IJ} = -1$ for $IJ = AP, PA$ and $+1$ otherwise. For all of our quark masses, the fits are excellent. For each correlation function, we define the corresponding pseudoscalar decay constant:

$$\begin{aligned} f_P^{IJ} &\equiv \frac{m_1+m_2}{M_{IJ}^2}\sqrt{\mathcal{Z}_{IJ}}, \quad IJ = PP, PP{-}SS \\ f_P^{IJ} &\equiv Z_A\frac{\sqrt{\mathcal{Z}_{IJ}}}{M_{IJ}}, \quad IJ = AA, J^LJ^L \\ f_P^{IJ} &\equiv \sqrt{Z_A\mathcal{Z}_{IJ}\frac{m_1+m_2}{M_{IJ}^3}}, \quad IJ = AP, PA\,, \end{aligned} \tag{5}$$

where, in our conventions, $f_\pi = 131\,\mathrm{MeV}$. The point of considering these three definitions is that they differ in their discretization errors. In fact, we expect these differences to be at most equal to the mass-dependent discretization errors identified in $Z_A(m_1, m_2)$. Indeed, f_P^{PP}/f_P^{AA} is simply $Z_A(m_1, m_2)/Z_A(0,0)$ to the extent that the fits to the continuum-limit parametrizations of Eq. (4) do not modify the relative discretization errors in the amplitudes $\mathcal{Z}_{IJ}$; that ∇_0 applied on $G_{A_0P}(t)$ yields a value of the pseudoscalar mass which is the same as the one determined by the fits; that finite-volume effects do not distort the various correlation functions differently. And under these same conditions, all other ratios of decay constants should be less than or equal to f_P^{PP}/f_P^{AA}. Moreover, the correlation functions are affected by topological zero modes differently. In particular, $PP - SS$ and $J_0^L J_0^L$ are free of zero modes. Differences at small quark masses thus give a measure of zero-mode contamination.

In Fig. 10 we plot f_P^{IJ} versus M_{IJ}, for all IJ. No statistically significant difference in the masses obtained from the various correlation functions is observed. At low quark mass this indicates that there is no evidence for zero-mode contamination in our fits. At high quark mass, the agreement is reassuring but not significant as discretization errors on the mass are determined by the action, which is the same for all correlation functions. That is not the case for the decay constant, where different correlation functions will induce different discretization errors. Indeed, we find that the difference increases as the quark mass is increased. For the "D_s", we find a variation of approximately 10% and it is 15% for the "η_c", which is entirely consistent with the results obtained from $Z_A(m_1, m_2)$, as anticipated. While significant, these variations do not indicate a major breakdown of the theory, even at $am_1 + am_2 = 1.5$. This is further confirmed by the fact that with a charm quark such that the corresponding "D_s" meson has a mass $\sim 1.95\,\mathrm{GeV}$ (i.e. $20\,\mathrm{MeV}$ below experiment), our "η_c" has a mass $\sim 2.93\,\mathrm{GeV}$ which is only $50\,\mathrm{MeV}$ (i.e. 2%) below experiment. Moreover, the preliminary value of f_{D_s} that we obtain is $267(15)(24)\,\mathrm{MeV}$, which is in good agreement with the most recent quenched calculation [17] and experimental measurement, $f_{D_s} = 285(19)(40)\,\mathrm{MeV}$ [18].

3.3. Charm quark summary

We have simulated the charm quark with overlap fermions on a lattice with $a^{-1} \sim 2\,\mathrm{GeV}$. We have investigated the effects of mass-dependent discretization errors on the axial Ward identity as well as on the pseudoscalar decay constant. We find that these effects are relatively small: 10% for the "D_s" and 15% for the "η_c". [3] We further find a value of f_{D_s} which is in good agreement with the latest quenched and experimental results. Thus, there is no sign of a major breakdown of the formalism even for bare quarks masses $am_q = 0.75$. Of course, these preliminary findings require fur-

[3] It should be noted, however, that these figures come from ratios of quantities in which some discretization errors may cancel.

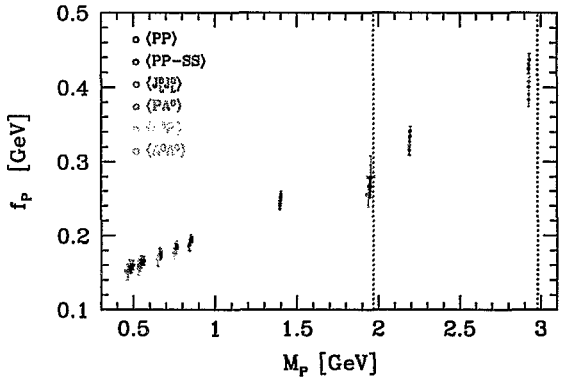

Figure 10. f_P vs. M_P as obtained from various 2-point functions. For clarity, only results for mesons composed of degenerate quarks are plotted, with the exception of our fiducial D_s meson. The vertical lines correspond, from left to right, to $P = D_s$ and $P = \eta_c$.

ther investigation and, in particular, the apparent smallness of discretization effects should be confirmed by simulations on finer lattices.

4. Weak matrix elements

4.1. Bare matrix elements

We have calculated the K^0-$\bar{K}^0$ mixing parameter B_K following the procedure detailed in [10,11]. B_K is defined as

$$B_K(\mu) = \frac{\langle \bar{K}^0 | O_{\Delta S=2}(\mu) | K^0 \rangle}{\frac{16}{3} M_K^2 F_K^2} \tag{6}$$

with ($\gamma_\mu^{L,R} = \gamma_\mu(1 \mp \gamma_5)$)

$$O_{\Delta S=2} = \bar{s}\gamma_\mu^L d \bar{s}\gamma_\mu^L d \tag{7}$$

The bare matrix element $\langle \bar{K}^0 | O_{\Delta S=2} | K^0 \rangle$ is extracted from the 3-point function

$$C_{JOJ}(x_0, y_0) = \sum_{\mathbf{x},\mathbf{y}} \langle J_0^L(x) O^{bare}_{\Delta S=2}(0) J_0^L(y) \rangle \tag{8}$$

and the 2-point function

$$C_{JJ}(x_0) = \sum_{\mathbf{x}} \langle J_0^L(x) \bar{J}_0^L(0) \rangle \tag{9}$$

which are both free of unphysical zero modes [19].

The large temporal extent of our lattice allows us to choose ranges $10 \leq x_0/a \leq 20$ and $44 \leq y_0/a \leq 54$ for the kaon source and sink, which are both safely in the asymptotic region $x_0 \gg a$, $y_0 \ll T$ and for which backward contributions due to the toroidal lattice geometry are negligible. As a consistency check, we have verified that within these ranges the pseudoscalar meson mass extracted from $C_{JOJ}(x_0, y_0)$ agrees very well with the ones extracted from various 2-point functions (cf. Section 2).

We have also computed the bag parameters $B_{7/8}^{3/2}$ of the electroweak penguin operators in the $\Delta I = 3/2$ channel of the $\Delta S = 1$ effective Hamiltonian. Following the convention of [20], we define

$$B_7^{3/2}(\mu) = \lim_{m \to 0} \frac{\langle \pi^+ | O_7^{3/2}(\mu) | K^+ \rangle}{\frac{2}{3} \langle \pi^+ | P(\mu) | 0 \rangle \langle 0 | P(\mu) | K^+ \rangle} \tag{10}$$

$$B_8^{3/2}(\mu) = \lim_{m \to 0} \frac{\langle \pi^+ | O_8^{3/2}(\mu) | K^+ \rangle}{2 \langle \pi^+ | P(\mu) | 0 \rangle \langle 0 | P(\mu) | K^+ \rangle} \tag{11}$$

where $O_7^{3/2}$ is given by

$$O_7^{3/2} = \bar{s}\gamma_\mu^L d(\bar{u}\gamma_\mu^R u - \bar{d}\gamma_\mu^R d) + \bar{s}\gamma_\mu^L u \bar{u}\gamma_\mu^R d \tag{12}$$

and $O_8^{3/2}$ is the corresponding color-mixed operator. We work in the $SU(3)_V$ limit $m_u = m_d = m_s$, in which all eye contractions cancel.

In contrast to B_K, finding appropriate sources to cancel all zero-mode contributions is not straightforward for $B_{7/8}^{3/2}$ due to the L-R structure of the operator. For this preliminary study, we therefore choose to simply report results obtained with pseudoscalar sources on the 3-point function

$$C_{7/8}(x_0, y_0) = \sum_{\mathbf{x},\mathbf{y}} \langle P(x) (O_{7/8}^{3/2})^{\text{bare}}(0) \bar{P}(y) \rangle \tag{13}$$

and the 2-point function

$$C_{PP}(x_0) = \sum_{\mathbf{x}} \langle P(x) \bar{P}(0) \rangle \tag{14}$$

and postpone a more careful investigation of this issue to a future publication.[4]

We identify nice plateaus in $C_{7/8}(x_0, y_0)$ in the range $18 \leq x_0/a \leq 23$ and $41 \leq y_0/a \leq 46$. In

[4]Pseudoscalar sources are not the optimal choice, since they allow for $1/m^2$ divergences in the 3-point functions.

this region, the mass extracted from the 3-point function agrees very well with the mass extracted from various 2-point functions (cf. Section 2).

4.2. Non-perturbative renormalization

We perform all renormalizations non-perturbatively in the RI/MOM scheme following [21]. Thus, we fix gluon configurations to Landau gauge and numerically compute appropriate, amputated forward quark Green functions with legs of momenta p. The renormalization of B_K is detailed in [11]. In order to renormalize $B_{7/8}^{3/2}$, we calculate the renormalization constants of a full set of dimension 6, 4-flavor operators in the basis suggested by [22]. In this basis, $O_7^{3/2}$ renormalizes as Q_2^+ and $O_8^{3/2}$ as $-2Q_3^+$. These 2 operators mix among each other but chiral symmetry protects them from mixing with other operators. The renormalization condition violates chiral symmetry at low p^2, but we found, that the violation is tiny.

The renormalization pattern for the B parameters is given by

$$\begin{pmatrix} B_7^{3/2} \\ B_8^{3/2} \end{pmatrix}^{\mathrm{RI}}(\mu) = \begin{pmatrix} Z_{77} & Z_{78} \\ Z_{87} & Z_{88} \end{pmatrix}^{\mathrm{RI}}(\mu) \begin{pmatrix} B_7^{3/2} \\ B_8^{3/2} \end{pmatrix}^{\mathrm{bare}} \tag{15}$$

In order to determine the $Z_{ij}^{\mathrm{RI}}(\mu)$ we define

$$\mathcal{R}_{ij}^{\mathrm{RI}}(\mu) = \lim_{m\to 0} \left. \frac{\mathrm{Tr}(P_S \Gamma_S(p^2,m))^2}{\mathrm{Tr}(P_i \Gamma_j(p^2,m))} \right|_{p^2=\mu^2} \tag{16}$$

where $\Gamma_i(p^2,m)$ is the amputated Green function of the operator $O_i^{3/2}$ and P_i the corresponding projector (cf. [22]). After performing an appropriate chiral extrapolation, we must isolate the "perturbative part" of this ratio to get the renormalization constant. In order to do this, we fit the matrix $\mathcal{R}^{\mathrm{RI}}(\mu)$ to the form

$$\begin{aligned} \mathcal{R}_{ij}^{\mathrm{RI}}(\mu) &= \cdots + \frac{A_{ij}}{\mu^4} + \frac{B_{ij}}{\mu^2} + Z_{ij}^{\mathrm{RI}}(\mu) \\ &\quad + C_{ij} \times (a\mu)^2 + \cdots \end{aligned} \tag{17}$$

where the running of $Z_{ij}^{\mathrm{RI}}(\mu)$ is given by NLO continuum perturbation theory. The $1/\mu^2$ and $1/\mu^4$ terms are motivated by the OPE in $1/p^2$ of Eq. (16), while the term $\propto (a\mu)^2$ takes into account leading order discretization effects.

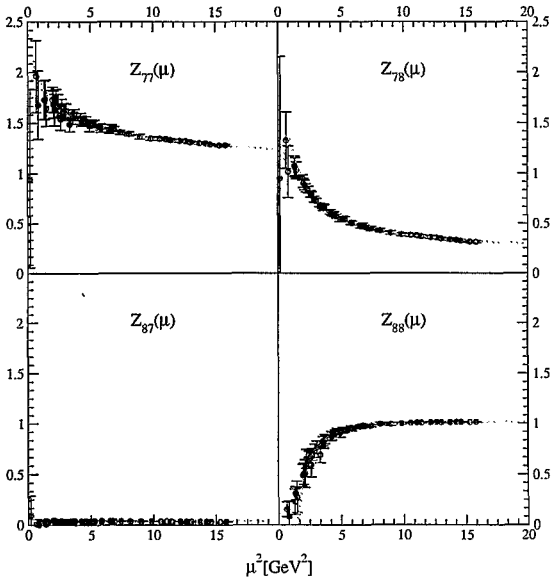

Figure 11. The coefficient matrix $\mathcal{R}_{ij}^{\mathrm{RI}}$ vs. μ. One can see, that the data are very well described by Eq. (17).

In Fig. 11 the $\mathcal{R}_{ij}^{\mathrm{RI}}(\mu)$ are shown together with fits of the form Eq. (17) in a range $\mu \in [\sqrt{2}, 3]$ GeV. The fit describes the data very nicely even far outside the fit range and is stable against addition of extra terms and variations in the fit range. Some of the fit parameters have numerically found to be consistent with 0 and have been eliminated.

4.3. Physical results

In Fig. 12 we show the renormalized value of B_K in the $\overline{\mathrm{MS}}$-NDR scheme at 2 GeV. We have performed both a linear and a chiral log fit of the form

$$B_K = B\left(1 - 6\left(\frac{M}{4\pi F}\right)^2 \ln\frac{M}{\Lambda_B}\right) \tag{18}$$

At the physical point, the result of both fits is virtually indistinguishable and we obtain $B_K^{\overline{\mathrm{MS}}\text{-NDR}}(2\mathrm{GeV}) = 0.61(7)$, where the error is statistical only. This result is compatible both

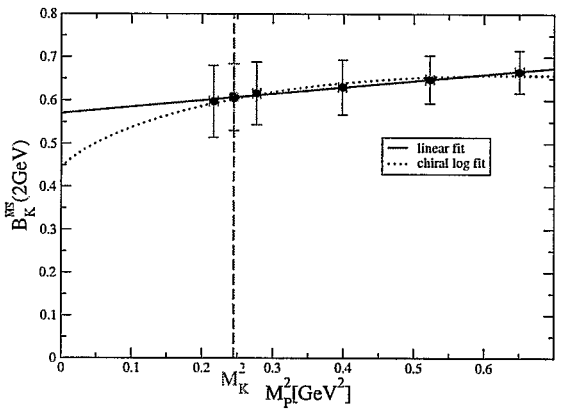

Figure 12. $B_K^{\overline{\text{MS}}\text{-NDR}}(2\text{GeV})$ vs. the pseudoscalar meson mass. The continuous line gives the result of a linear fit and the dotted line of a chiral log fit of the form Eq. (18).

with our earlier result from smaller lattices [11] and with a recent determination by the MILC collaboration [15].

In Fig. 12 we plot the renormalized value of $B_{7/8}^{3/2}$ in the $\overline{\text{MS}}$-NDR scheme at 2 GeV as a function of M_P^2. We postpone the study of this mass

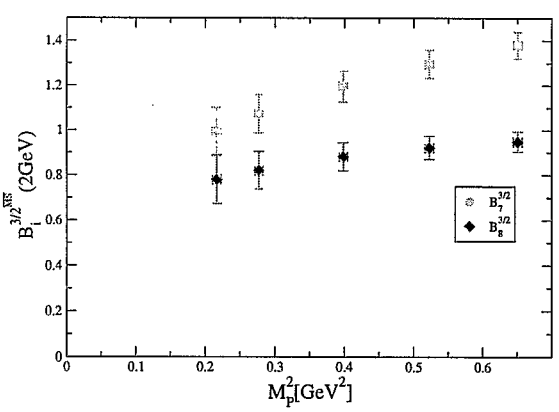

Figure 13. $\left(B_{7/8}^{3/2}\right)^{\overline{\text{MS}}\text{-NDR}}$ (2GeV) vs. the pseudoscalar meson mass.

dependence to a later publication.

REFERENCES

1. D.B. Kaplan, Phys. Lett. B288 (1992) 342.
2. Y. Shamir, Nucl. Phys. B406 (1993) 90.
3. R. Narayanan and H. Neuberger, Nucl. Phys. B443 (1995) 305.
4. R. Narayanan and H. Neuberger, Nucl. Phys. B412 (1994) 574.
5. H. Neuberger, Phys. Lett. B417 (1998) 141.
6. P.H. Ginsparg and K.G. Wilson, Phys. Rev. D25 (1982) 2649.
7. M. Lüscher, Phys. Lett. B428 (1998) 342.
8. L. Giusti, C. Hoelbling and C. Rebbi, Phys. Rev. D64 (2001) 114508.
9. L. Giusti, C. Hoelbling and C. Rebbi, Nucl. Phys. Proc. Suppl. 106 (2002) 739.
10. N. Garron, L. Giusti, C. Hoelbling, L. Lellouch and C. Rebbi, Nucl. Phys. Proc. Suppl. 119 (2003) 356.
11. N. Garron, L. Giusti, C. Hoelbling, L. Lellouch and C. Rebbi, hep-ph/0306295.
12. S.J. Dong, T. Draper, I. Horvath, F. Lee, K. Liu, N. Mathur and J. Zhang, hep-ph/0306199.
13. S.J. Dong, T. Draper, I. Horvath, F. Lee, K. Liu, N. Mathur and J. Zhang, hep-lat/0304005.
14. T.W. Chiu and T.H. Hsieh, hep-lat/0305016.
15. T. DeGrand, hep-lat/0309026.
16. K.F. Liu, hep-lat/0206002.
17. A. Juttner and J. Rolf (ALPHA), Phys. Lett. B560 (2003) 59.
18. A. Heister et al. (ALEPH), Phys. Lett. B528 (2002) 1.
19. L. Giusti, C. Hoelbling, M. Lüscher and H. Wittig, Comp. Phys. Comm. 153 (2003) 31.
20. L. Lellouch and C.J.D. Lin (UKQCD), Nucl. Phys. Proc. Suppl. 73 (1999) 312.
21. G. Martinelli, C. Pittori, C.T. Sachrajda, M. Testa and A. Vladikas, Nucl. Phys. B445 (1995) 81.
22. A. Donini, V. Gimenez, G. Martinelli, M. Talevi and A. Vladikas, Eur. Phys. J. C10 (1999) 121.